Traveling glycolytic waves induced by a temperature gradient and determination of diffusivities for dense media

A. Yu. Verisokin, D. V. Verveyko, and E. B. Postnikov*
Department of Theoretical Physics, Kursk State University, Radishcheva Street, 33, 305000, Kursk, Russia
(Received 28 July 2011; revised manuscript received 17 June 2012; published 30 July 2012)

Here we consider the spatially extended model incorporating the temperature-dependent autocatalytic coefficient into the Merkin-Needham-Scott version of the Selkov system and show that this model with temperature gradient quite reasonably explains the experimentally detected traveling glycolytic nonstationary waves, which can be attributed as kinematic ones. Additionally, we analyze the influence of possibly incorporating diffusion terms into the equations. It is shown that the value of diffusivity influences the timetable for the birth of new wave and their further evolution. This result could be used as a method for the determination of diffusivity.

DOI: 10.1103/PhysRevE.86.012901 PACS number(s): 82.39.−k, 87.10.Ed

I. INTRODUCTION

Biological extracts fixed in dense media (e.g., gels) are widely used in experimental research [1]. At the same time, the principal problem of modeling experiment-based reaction-diffusion patterns in such media is the determination of diffusivities. The problem is connected with the gel structure: the gel structure has a complex microstructure providing multiple backscattering that hinders the application of optical and single-particle tracing techniques. There are several known methods which partially overcome the mentioned difficulties, such as nuclear magnetic resonance or fluorescence correlation spectroscopy (see, e.g., Refs. [2,3] and references therein). However, the application of these methods remains complex. Thus, this motivates researchers to seek new approaches for the determination of diffusion coefficients in dense media based on the analysis of the dynamical processes of the reacting components filling the gel.

As an example, we consider the results of the extensive experimental studyby Mair *et al.* [4] devoted to the spatiotemporal dynamics of glycolytic reactions in a gel-fixed yeast extract. They found that a temperature gradient applied to this system results in traveling waves propagating from the warm side of the gel to the cold one.

In our previous article [5] we have shown that principal features of temperature-dependent glycolytic oscillations in a closed chemical reactor [4] can be reproduced within a simple model which incorporates the temperature-dependent autocatalytic coefficient,

$$\beta(T) = \beta_0 \exp(-k/T), \tag{1}$$

into the Merkin-Needham-Scott version of the Selkov system:

$$\frac{dx}{dt} = \nu - \alpha x - \beta(T) x y^2, \tag{2}$$

$$\frac{dy}{dt} = -wy + \alpha x + \beta(T) x y^2, \tag{3}$$

$$\frac{dv}{dt} = -\varepsilon v. \tag{4}$$

Here the variables x and y are the concentrations of substrate (adenosine-5′-triphosphate, ATP) and product (adenosine diphosphate, ADP), ν is the initial quantity of substrate within the vessel, and the constant w determines the outflow from the sphere of reaction, i.e., the elimination of ADP from the first, phosphofructokinase-catalyzed, step of glycolysis and not a physical outflux from the vessel.

Reference [5] deals with the time evolution of concentration only. The goals of the presented work are the following: (i) to show that the system, Eqs. (2)–(4), extended by diffusion terms allows us to reproduce the spatiotemporal behavior studied previously [4] and (ii) to discuss a method for the determination of diffusivities in dense gels based on temperature-dependent reactions.

Note that in the considered case we deal with the experimental situation, which crucially differs from that of a set of previous studies [6–8], where the open spatial reactor has been considered. Thus, the finite diffusion was a controlling transport factor directly coupled with the spatially nonuniform substrate or product exchange with an outer media. In that case the boundary conditions on the penetrable reactor's bottom were taken into account. Conversely, here we consider the closed reactor, i.e., fixed nonpenetrable boundary conditions. Therefore, the whole process is governed by parameters of reaction and by a diffusion strictly inside the reactor.

II. RESULTS

A. Kinematic waves

First of all, we need to remind the reader that the agarose gel (in which yeast extract is fixed) is a sufficiently dense medium. As a consequence, the dynamical behavior has an extremely weak dependence on the diffusion (the case of larger diffusivities will be discussed in Sec. II B of this work). This is argued and discussed in Ref. [7]. Although the experimental setup modeled in Ref. [7] contains an open chemical reactor in constrast to the closed one used in Ref. [4], the gels in both reactors are identically prepared under the same experimental conditions.

For this reason the spatially distributed temperature dependence can be incorporated via the simple inclusion of the spatial coordinate r into equality (1). As has been shown in Ref. [5], the system of Eqs. (2)–(4) is actually two-dimensional since Eq. (4) has the explicit solution $v(t) = v_0 \exp(-\varepsilon t)$, which can be substituted into Eq. (2). Introducing the variable

*postnicov@gmail.com

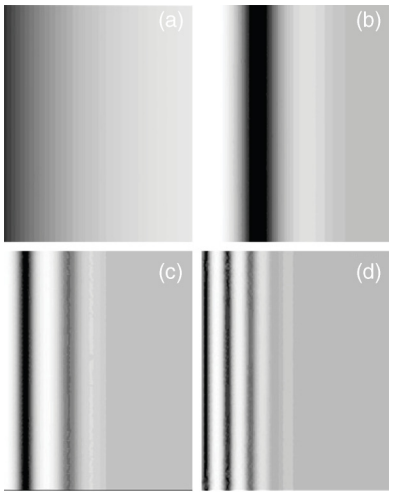

FIG. 1. Four sequential pictures representing the time evolution of traveling waves (compare with Fig. 8 in Ref. [4]). Darker regions correspond to the larger y concentration. Shortly after the beginning of the reaction (a) the traveling solitary wave is formed (b). (c) With time lapse, one can see the new wave hurries the first one. (d) The process of multiplication of the number of waves continues further during the reaction. A detailed space-time picture of wave emergence and distribution is shown in the supplementary video [10].

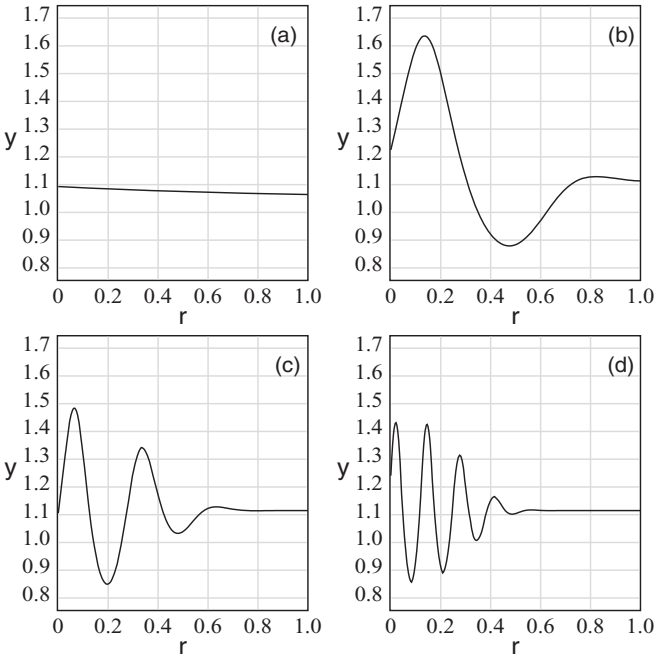

FIG. 2. Horizontal cross sections of four wave patterns presented in the Fig. 1 demonstrating the spatial distribution of concentration for these time moments. All quantities are dimensionless.

ξ in such a way that

$$x = \frac{z_0 w - \nu + w\xi + \dot{\xi}}{w}, \quad y = \frac{\nu - \dot{\xi}}{w},$$

where

$$z_0 = \frac{w^3 v + \beta\nu^3 + \alpha\nu w^2}{\beta\nu^2 w + \alpha w^3}$$

is the total equilibrium concentration of reagents, we represent Eqs. (2) and (3) in the form of a single second-order differential equation (generalized Rayleigh equation):

$$\ddot{\xi} + \lambda\dot{\xi} + \lambda''\dot{\xi}^2 + \lambda'\dot{\xi}^3 + [\alpha w + \beta\Omega^2(1 - \nu^{-1}\dot{\xi})^2]\xi = 0,$$

with the coefficients $\lambda = [3\nu^2\beta + w^2(w + \alpha) - 2\beta\nu w z_0]/w^2$, $\lambda' = \beta/w^2$, $\lambda'' = \beta(z_0 w - 3\nu)/w^2$, and $\omega = \nu/\sqrt{w}$.

It is known that oscillating solutions of the generalized Rayleigh equation are governed by two principal parameters: λ, a sign of which determines the transition from the steady state ($\lambda > 0$) regime to the oscillating ($\lambda < 0$) regime via the Hopf bifurcation $\lambda = 0$ and ω, which is a frequency of weak, nonlinear, self-sustained oscillations (i.e., near the Hopf bifurcation).

In the considered case the above-mentioned two parameters are the following coordinate-dependent functions

$$\lambda[T(r)] = \frac{\nu^4\beta[T(r)]2 - 2\nu^2 w^2(w + \alpha)\beta[T(r)] + w^4\alpha(w + \alpha)}{\alpha w + \nu^2\beta[T(r)]}, \tag{5}$$

$$\omega[T(r)] \approx \left[\alpha w + \beta[T(r)]\frac{\nu^2}{w}\right]^{1/2}, \tag{6}$$

TABLE I. Dependence of time of nth wave's birth on diffusivity. The last column presents the characteristic period of oscillations at the left border. The waves which emerge but vanish after a certain time interval are marked by asterisks.

D	$n = 1$	$n = 2$	$n = 3$	$n = 4$	$n = 5$	$n = 6$	T_0
0–10^{-6}	0.7	5.2	18.4	31.7	44.9	58.2	4.39
5×10^{-6} to 10^{-5}	0.7	5.2	18.5	31.8	45	58.5	4.40
5×10^{-5}	0.7	5.2	18.6	32	45.6		4.41
7×10^{-5} to 9×10^{-5}	0.7	5.2	18.7	32.2	50.3		4.44
1×10^{-4}	0.7	5.3	18.7	36.7			4.47
3×10^{-4}	0.8	5.3	23.5	41.9*			4.53
5×10^{-4}	0.8	5.4	28.4*				4.59
7×10^{-4}	0.8	5.4	33.2*				4.63
10^{-3}	0.8	5.4	8*				4.66
3×10^{-3}	0.8	10.4*					4.71
5×10^{-3}	0.8						4.74

where the notation $T(r)$ highlights the previously mentioned co-ordinate dependence, which originates from the temperature nonhomogeneity. The approximate equality is used in Eq. (6) since this equation represents the "frequency factor," which practically coincides with the frequency in the weak nonlinear case.

We simulate the one-dimensional temperature gradient described in Ref. [4] substituting $T = a - br$ into the system of Eqs. (1)–(4). The values $a = 296$ and $b = 0.2$ correspond to the linear change of temperature from $T_{\max} = 23\,^{\circ}\mathrm{C}$ down to $T_{\min} = 3\,^{\circ}\mathrm{C}$ along $r = [0,1]$ (dimensionless units). Other parameters are $w = 2$, $\nu = 2.23$, $\alpha = 0.24$, $\varepsilon = 0.009$, $\beta_0 = 5.53 \times 10^6$, and $k = 4.73 \times 10^3$. Motivated by the experimental setup with impenetrable boundaries, we use the null-flux boundary conditions for both variables x and y.

Results of the simulation using FLEXPDE software [9] are presented in Figs. 1 and 2 and as a supplementary movie [10]. One can compare Fig. 1 with Fig. 8 in Ref. [4] and see quite a good resemblance between both pictures: the emergence of a wave and, subsequently, of wave trains traveling along the direction of the temperature gradient (for details of the time evolution, see the supplementary movie [10]).

Since there are no spatial derivatives in Eqs. (2)–(4), these waves should be classified as kinematic ones [11]. In other words, they originate from various frequencies of oscillations (6) at adjacent points. This condition is fulfilled in the considered system. This generates a phase gradient in the oscillations that is visible as a traveling wave. Additionally, the continuous frequency distribution leads to incomparable periods of oscillations. As a result, with time lapse one can see simultaneously more and more concentration maxima in the spatial interval, i.e., visible wave trains.

Furthermore, all traveling waves vanish on the right-hand side of the reactor: the right half of all the panels in Fig. 1 shows a uniform distribution that also corresponds to the experimental Fig. 8 in Ref. [4]. The explanation of this fact is based on Eq. (5). The colder half of the reactor due to Eq. (1) gives values of β, substitution of which into Eq. (5) leads to $\lambda > 0$, i.e., stable steady states.

B. Effect of diffusion

Now let us consider the case of small but finite diffusivities, D, equal for both reagents. This equality is based on the fact that a diffusion coefficient is determined by the viscosity of the milieu and the sizes of the molecules, but the last ones are practically equal for similar molecules such as ATP and ADP [12]. Other possible factors that could have an effect on the various diffusion rates (interactions with other metabolites) are negligible for the considered experimental conditions of dense gel. Concerning the experimental procedures, such as gel-fixed extract preparation, reaction stimulation, etc., they were the same in both Refs. [6] and [4] (only boundary conditions were different). Results of the analysis presented in Ref. [6] completely confirm the equality of the diffusion coefficients.

In this case the terms $D\partial_r^2 x$ and $D\partial_r^2 y$ will be added to the right-hand sides of Eqs. (2) and (3), correspondingly. The numerical simulation shows that a growth of diffusivity leads to qualitative change in the waves' behavior. Two main effects are observed: (i) the time interval between the appearance of subsequent waves increases and (ii) the process of multiplication for the number of waves stops after a certain time. Table I summarizes the results about the moments t_n, when the next wave (sorted by its number n) appears for the first time. During the observation time, for $D \leqslant 10^{-5}$, the function $n(t_n)$ can be fitted as a linear one for the waves from the third to the sixth. The interpretation of this fact is a direct outcome of the kinematic mechanism described above: the frequency of local oscillations decays from the left to the right border due to the temperature gradient; therefore a new wave

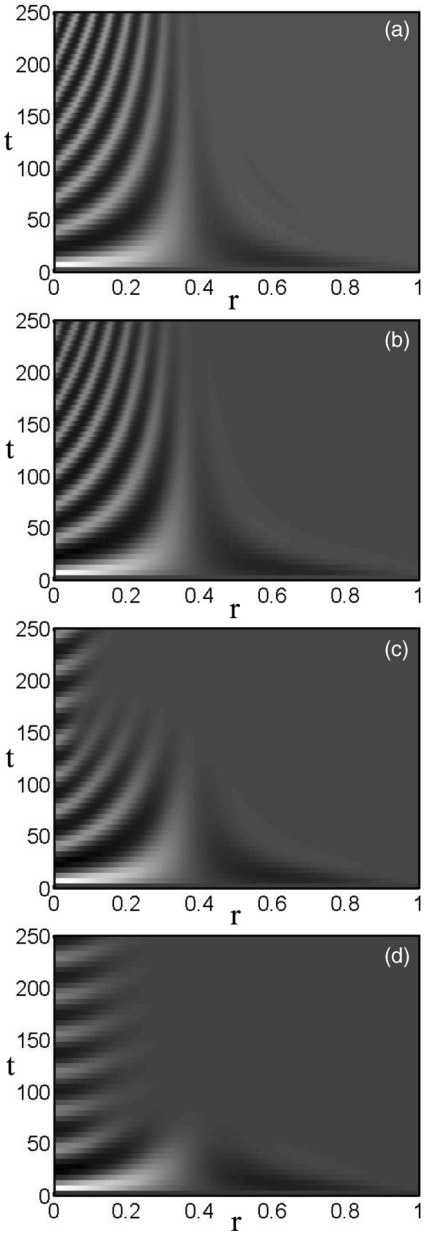

FIG. 3. The space-time plots of traveling waves emerging for the glycolytic system with various dimensionless diffusivities (these pictures can be considered as the continuous merging instant horizontal slices of the two-dimensional spatial reactor, which is seen from above in Fig. 1): (a) , (b) $D = 10^{-6}$, (c) $D = 10^{-5}$, and (d) $D = 10^{-4}$. Other model parameters are the same as the ones listed in Sec. II A.

appears after each full period while the previous oscillation on the right-hand side is not yet completed.

The growth of diffusivity leads to synchronization of the local oscillation periods. As a result, $n(t_n)$ up to $D \approx 10^{-4}$ grows almost linearly again (with a larger slope corresponding to a larger mean period of oscillations) but stops after a finite number of waves' births, i.e., the moment when the complete frequency synchronization occurs. As a confirmation of this fact we can use the growth of the oscillation period at the left border for the regime of final stable oscillations (last column in the Table I). This explanation also confirms the fact that the last multiwave for the interval $D = 3 \times 10^{-4}$ to 3×10^{-3} emerges and then vanishes (corresponding times are marked by asterisks in Table I). This means that the fast process of wave multiplication originated from local oscillations is overlapped further by more slow diffusion. Such behavior is illustrated in the next section by the space-time plots, where clusters of synchronization are shown.

The results presented in Table I also reveal features connected with the advantages and disadvantages of this method for the determination of diffusion coefficients. Numerical simulations show that the criterion of the "number of waves emerging before process stabilization" is sufficiently stable with respect to a variation of D up to a half-order of the magnitude. This is demonstrated via the representation of data in Table I. For each interval of diffusivities, placed in the first column, there are presented moments of emergence of wave's number indicated in the title row. The last number in each row corresponds to the number of waves in a stable regime, i.e. there are no new births of waves and further places in the row are empty. At the same time, this stability bounds the exactness of the results by a high order of magnitude.

III. DISCUSSION AND OUTLOOK

The considered situation is close to the behavior studied in Ref. [13] for the case of the Belousov-Zhabotinsky reaction in weakly connected adjacent cells. As in the cited article, we can see the process of sequential entrainment of oscillations leading to the synchronized phase-diffusion waves for sufficiently large diffusivities.

However, in addition to Ref. [13], where only a unique coupling parameter has been used, our Fig. 3 allows us to explore the process of synchronization in more detail. The competition between the diffusive coupling and the initial nonuniformity of the local oscillation frequency distribution can proceed in two ways: Fig. 3(c) demonstrates emergence and growth of the synchronized oscillating cluster (see it at the left border starting from $t = 140$); Fig. 3(d), corresponding to the larger diffusivity, shows the situation when the diffusion process is too fast to form a synchronized cluster with definite borders. A characteristic time of diffusion across the region is comparable with the time of the kinematic wave's motion [as in Figs. 3(d)] or shorter.

To transform the discussed dimensionless values to the dimensional value, we fitted data on the periods [5] (the resulting scale coefficient is $T/T_{\text{dimensionless}} = 35 \pm 5$ min) and the dimensionless interval [0,1], which corresponds to the reactor's 35-mm diameter. The dimensional diffusion coefficient measured in mm^2/s can be obtained via the multiplication of the dimensionless values D used in this work by the numerical factor from the range 0.43–0.76.

Thus, analyzing Fig. 8 in Ref. [4] and comparing it with our Fig. 3 and our Table I we conclude that in the cited experiment the diffusivity has an order of no more than 10^{-5} mm^2/s. The observed waves are kinematic and all the conclusions of Sec. II A are fulfilled.

Finally, the strong interconnection between qualitative and quantitative pictures of the evolution and intervals of diffusivity of wave trains allows us to propose a method for the experimental determination of a diffusion coefficient in a dense gel. Since the principal conclusions are based on the interplay of the continuous frequency distribution and the synchronization due to a weak diffusive coupling, the outlook is not constrained by the concrete biochemical reaction. One can use general gel-fixed chemical reagents, which admit oscillatory reactions with a temperature-dependent period. Then, placing the chemical reactor under a temperature gradient, the birth and evolution of waves will be detected. The character of this temporal evolution provides data about the ranges of the desired diffusion coefficients.

[1] R. M. Ottenbrite and S. J. Huang, *Hydrogels and Biodegradable Polymers for Bioapplications* (American Chemical Society, Washington, DC., 1996).

[2] N. Fatin-Rouge, K. Starchev, and J. Buffle, Biophys. J. **86**, 2710 (2004).

[3] C. E. Muir, B. J. Lowry, and B. J. Balcom, New J. Phys. **13**, 015005 (2011).

[4] T. Mair, C. Warnke, K. Tsuji, and S. C. Müller, Biophys. J. **88**, 639 (2005).

[5] E. B. Postnikov, D. V. Verveyko, and A. Y. Verisokin, Phys. Rev. E **83**, 062901 (2011).

[6] A. Lavrova, S. Bagyan, T. Mair, M. J. B. Hauser, and L. Schimansky-Geier, BioSystems **97**, 127 (2009).

[7] A. I. Lavrova, L. Schimansky-Geier, and E. B. Postnikov, Phys. Rev. E **79**, 057102 (2009).

[8] E. B. Postnikov, A. Y. Verisokin, D. V. Verveyko, and A. I. Lavrova, Phys. Rev. E **81**, 052901 (2010).

[9] FLEXPDE, v. 5.0.22, applies Galerkin finite element methods, with triangular mesh. The implicit backward difference method with adaptive mesh and time step refinements is used. The default estimated relative spatial and temporal error is 0.002.

[10] See Supplemental Material at http://link.aps.org/supplemental/10.1103/PhysRevE.86.012901 for presenting time evolution of traveling waves.

[11] J. Ross, S. Müller, and C. Vidal, Science **248**, 460 (1988).

[12] D. L. Nelson, A. L. Lehninger, and M. M. Cox, *Lehninger Principles of Biochemistry* (Freeman, New York, 2008).

[13] O.-U. Kheowan, E. Mihaliuk, B. Blasius, I. Sendiña-Nadal, and K. Showalter, Phys. Rev. Lett. **98**, 074101 (2007).